Biosensors and Bioelectronics 129 (2019) 93–99

Contents lists available at ScienceDirect

Biosensors and Bioelectronics

journal homepage: www.elsevier.com/locate/bios

Exploiting electrostatic shielding-effect of metal nanoparticles to recognize uncharged small molecule affinity with label-free graphene electronic biosensor

Cheng Wang[a,b,c,d,*,1], Weixiang Ye[a,b,e,f,1], Yijun Li[a,b,g], Yibo Zhu[g], Qiao Lin[g], Miao He[a,b,*]

[a] Center for Sensor Technology of Environment and Health, School of Environment, Tsinghua University, Beijing 100084, China
[b] State Key Joint Laboratory of Environmental Simulation and Pollution Control, Tsinghua University, Beijing 100084, China
[c] Department of Artificial Intelligence, College of Electronic and Communication Engineering, Tianjin Normal University, Tianjin 300387, China
[d] Tianjin Key Laboratory of Wireless Mobile Communications and Power Transmission, Tianjin Normal University, Tianjin 300387, China
[e] Institute of Physical Chemistry, Johannes Gutenberg University of Mainz, Mainz D-55128, Germany
[f] Graduate School of Excellence Materials Science in Mainz (MAINZ), Mainz D-55128, Germany
[g] Department of Mechanical Engineering, Columbia University, New York, NY 10027, United States

ARTICLE INFO

Keywords:
Uncharged small molecule
Competitive affinity
Metal nanoparticle analogue
Electrostatic shielding-effect
Graphene field-effect transistor biosensor

ABSTRACT

Label-free electronic biosensors as the non-electrochemical analytical tools without requirement of sophisticated instrumentation have become attractive, although their application in competitive affinity sensing of uncharged small molecules is still hindered by a difficulty in the development of competing analogues. To break through this bottleneck, we report a novel analogue made by epitope-modified metal nanoparticles to enable the electronic signaling of small-molecule analyte recognition via competitive affinity. While the electronic signaling capability of metal nanoparticle analogues is demonstrated by a graphene field-effect transistor bioassay of small-molecule glucose as a proof-of-principle, interestingly, we discover a new electronic signaling mechanism in the metal nanoparticle affinity, different to the intuitive charge accumulation expectation. On the basis of Kelvin-probe force microscopic potential characterization and theoretical discussion, we fundamentally elucidated the signaling mechanism as a seldom used electrostatic shielding-effect, that is, in the analogue-receptor affinity, metal nanoparticles with the charge density lower than receptor biomolecules can reduce the collective electrical potential via charge dispersion. Further consider the convenient epitope-modifiability of metal nanoparticles, the easy-to-develop analogues for diverse target analyte might potentially be predictable in the future. And the application of label-free electronic biosensors for the competitive affinity bioassay of range-extended small molecules may thus be promoted based on the electrostatic shielding-effect.

1. Introduction

Label-free electronic biosensors as the convenient non-electrochemical analytical tools have been showing merits in novel biochemical analysis, owing to the simplified implementation and instrumentation (Zhang and Lieber, 2015). By means of receptor functionalization, the susceptibility of sensitive materials can directly transduce the affinity of target objects into electronic signals without the assistance of electrochemical reactions and Faradaic current (Luo and Davis, 2013). And the sensor outputs, either manifested by basic potentiometric signal or amplified into transistor conductivity, make the bioinformation detectable with simple peripherals and settings.

However, the direct affinity biosensing is usually limited to charged macromolecules (e.g., protein and nucleic acid species), not available for most of the small-molecule analytes lacking of ionizable groups and electric charges (Zeng et al., 2014). Although a competitive affinity sensing principle that enables the electronic signaling via competitive analogue-receptor affinity has been demonstrated (Li et al., 2019; Zayats et al., 2006), to this day, only a few small molecules with suitable aptamers and oligonucleotide competing analogues have been successfully detected, due to a primary difficulty in the analogue development (Li et al., 2017; Wang et al., 2015). For these reasons, novel easy-to-develop analogues are eagerly desired to overcome the practicability limitation in competitive affinity electronic biosensors.

* Corresponding authors at: Center for Sensor Technology of Environment and Health, School of Environment, Tsinghua University, Beijing 100084, China.
E-mail addresses: cwang@tsinghua.edu.cn (C. Wang), hemiao@tsinghua.edu.cn (M. He).
[1] These authors contributed equally to this work.

https://doi.org/10.1016/j.bios.2018.12.051
Received 19 September 2018; Received in revised form 10 December 2018; Accepted 28 December 2018
Available online 09 January 2019
0956-5663/

In this work, we first report a novel analogue made by metal nanoparticles, which may open up the customizable analogue development via proper epitope-modification corresponding to target small molecules. While metal nanoparticles have been widely used in plasmonic and electrochemical biosensing (Sperling and Parak, 2010), to our knowledge, their use in label-free electronic biosensing as the competing analogues is rarely investigated as yet. Here, we conduct a label-free glucose bioassay based on graphene field-effect transistor (GFET) electronic biosensor as a proof-of-principle. By employing silver nanoparticles with glucoside-epitopes as the analogue, which is capable to bind with the glucose receptor lectin concanavalin A (ConA) (Cummins et al., 2013), the competitive affinity electronic biosensing of glucose is experimentally demonstrated with a detection limit about 3.0 μg dL^{-1} (ca. 165.3 nM), not inferior to commercial instruments.

Although an individual glucometer device per se is somewhat a cliché, more importantly, glucose as a thoroughly investigated model small molecule provides reliable evidence supporting our discussion on the newly discovered electronic signaling mechanism of metal nanoparticle analogue. We observe that silver nanoparticles binding on the self-assembly monolayer (SAM) of ConA receptor induce an unexpected *n*-type doping, whereas silver nanoparticles also take negative charges same to ConA. This result seems to violate the common understanding that the interfacial accumulation of negative charges may induce opposite *p*-type doping via electric field-effect (Fu et al., 2016). To confirm this mechanism, we conduct the theoretical analysis of electrical potential distribution in GFET, and fundamentally elucidate that the metal nanoparticles binding on SAM reduce the collective electric negativity manifestation via the electrostatic shielding-effect (Molinaro et al., 2016), by which excessive receptor charges are dispersed into the metal nanoparticles with relatively tenuous charge matrix. As the Kelvin probe force microscopic (KPFM) characterization also supplies direct evidence supporting our elucidation, we believe that metal nanoparticle analogues are capable to enable the competitive affinity electronic sensing of uncharged analytes. The multiple epitope-modifiability potential of metal nanoparticles may facilitate diverse competing analogue development in the future, and promote the application of label-free electronic biosensors for range-extended small molecules with biomedical significances.

2. Results and discussion

2.1. Sensor device

In pursuit of ideal sensing performances, we chose graphene, the most sensitive electronic material ever known (Novoselov et al., 2012), to fabricate the GFET sensor devices under a high-κ solid-gate configuration (Zhu et al., 2015). As the schematic shown in Fig. 1**a**, the sensitive unit made by monolayer chemical vapor deposition (CVD) graphene is gated by a planar metallic electrode through a 30 nm HfO_2 dielectric layer ($\varepsilon_{HfO_2} \approx 16$). And a microfluidic channel packages the GFET to achieve controllable liquid handling. The device fabrication details are provided in Supplementary Information (SI) Fig. S1. In brief, we adopted standard IC fabrication techniques to realize the tape-out of GFET devices in batch (Lerner et al., 2014). As shown in Fig. 1**b**, a little-scale batch of 48 devices manufactured on a 4-in. wafer performs the yield 100%, and possesses scalable production capability. These devices as one-time used disposable biosensors might be characteristically similar, which is beneficial to enhance the measurement reproducibility.

To avoid the errors caused by mechanical instability in electrical tests, the sensor devices with the overall size 1 cm × 1 cm were fixed on an electrical probe station to carry out all the tests (Fig. 1**c**). And the liquid introducing, changing and removal in experiments were also executed in situ by a syringe pump without device movement. As shown in Fig. 1**d**, the length and width of graphene sensitive unit are $L = 40$ μm and $W = 80$ μm, respectively. During the electrical tests, the current I_{ds} between drain and source electrodes, or the GFET conductivity $\sigma = (L/W)(I_{ds}/V_{ds})$, can be observed as the sensor output under the potentiostatic drain voltage V_{ds}.

2.2. Competitive affinity electronic biosensing principle

Our GFET sensor devices were functionalized by the ConA receptor to realize the recognition of glucose (Cummins et al., 2013), which is chosen as the representative analyte of uncharged small molecules. To competitively enable the electronic signaling of glucose affinity, the analogue has to possess ConA-binding sites similar to glucose. Consider the modifiability of metal nanoparticles, multiple methods could be employed to easily fabricate metal nanoparticle analogues via epitope immobilization (Sperling and Parak, 2010). As the ConA-binding epitopes of glucose are the hexose hydroxyls also existing in glucoside derivatives (Loka et al., 2015), dextran polymers consisting of glucoside monomers can provide the ConA-binding sites. Hereby, we synthesized the glucose-competing silver nanoparticles via a one-step hydrothermal route, in which the long-chain polyol dextran playing both the reducer and stabilizer roles directly reduces the silver diamminohydroxide precursor into the dextran-stabilized silver nanoparticles (DexAgNPs) (Wang et al., 2014; Ye et al., 2014; Zhang et al., 2014). The tethered long-chains with remnant glucoside epitopes supply the ConA-binding sites on DexAgNPs. In this work, DexAgNPs with the average diameter of 25 nm and zeta-potential $\xi \approx -25$ mV were chosen as the analogue. The satisfactory monodispersity and long-term stability in aqueous media preserve the analogue reliability in competitive affinity biosensing (see synthesis and quality characterization details in SI Figs. S2–S5).

As the competitive affinity biosensing principle designed in Fig. 2, the pristine graphene sensitive unit is adsorbed by pyrenebutyric acid N-hydroxysuccinimide ester (PBA-NHS) linker to immobilize the SAM of ConA receptor, and reversibly capture DexAgNPs (see **SI** for detailed protocol of functionalization). The atomic force microscopic (AFM) images in Fig. 2 present straightforward demonstration of DexAgNP capture. While DexAgNPs are sufficiently charged to maintain the colloidal stability as isolated metal conductors in aqueous solutions, we estimate that the DexAgNP-ConA affinity (from stage iii to iv) is capable to perturb the SAM potential and excite GFET responses. Thereby, the glucose competition compromising DexAgNP-ConA affinity (from stage iv to vi) may kinetically modulate the glucose concentration information onto the disappearance rate of DexAgNP signaling.

2.3. Electrical characterization and Electrostatic shielding-effect

To testify the electronic signaling capability of our DexAgNP analogue, as well as the validity of competitive affinity electronic biosensing (Fig. 2), we electrically characterized the GFET sensor in a 4-(2-hydroxyethyl)-1-piperazineethanesulfonic acid (HEPES) buffer solution (pH 7.4, ionic strength $I \approx 50$ mM consisting of 50 mM HEPES and 50 mM $NaNO_3$). As the GFET transport characteristic curves (σ vs. V_{gs}) shown in Fig. 3**a**, the shifts of Dirac voltage identifier (minimal σ point at $V_{gs} = V_{Dirac}$) clearly illustrate the electronic signaling during the reversible DexAgNP-ConA binding processes (corresponding to stage iii to v in Fig. 2). Concretely, the pristine GFET exhibiting $V_{Dirac}^{(i)} = 0.885$ V (stage i in Fig. 3**a**) suggests an original *p*-type doping from the puddles of ubiquitous contacting impurities (Chen et al., 2008). Then, the immobilization of nonionizable PBA-NHS linker leads to a slight *p*-type doping strengthening $V_{Dirac}^{(ii)} = 0.998$ V (stage ii), which is attributed to a few incidental impurities brought by the adsorption of pyrenyl basal plane on graphene (Sreeprasad and Berry, 2013). After the ConA immobilization forming SAM, a distinct positive shift $V_{Dirac}^{(iii)} = 1.646$ V appears (stage iii). Since ConA molecules do not directly contact on graphene surface, the *p*-type hole doping is induced by the negative protein ionization charges via electric field-effect (Locke et al., 2014; Pace et al., 2009). After the DexAgNP capture, an *n*-type doping $V_{Dirac}^{(iv)} = 1.383$ V (stage iv) demonstrates the electronic signaling of DexAgNPs

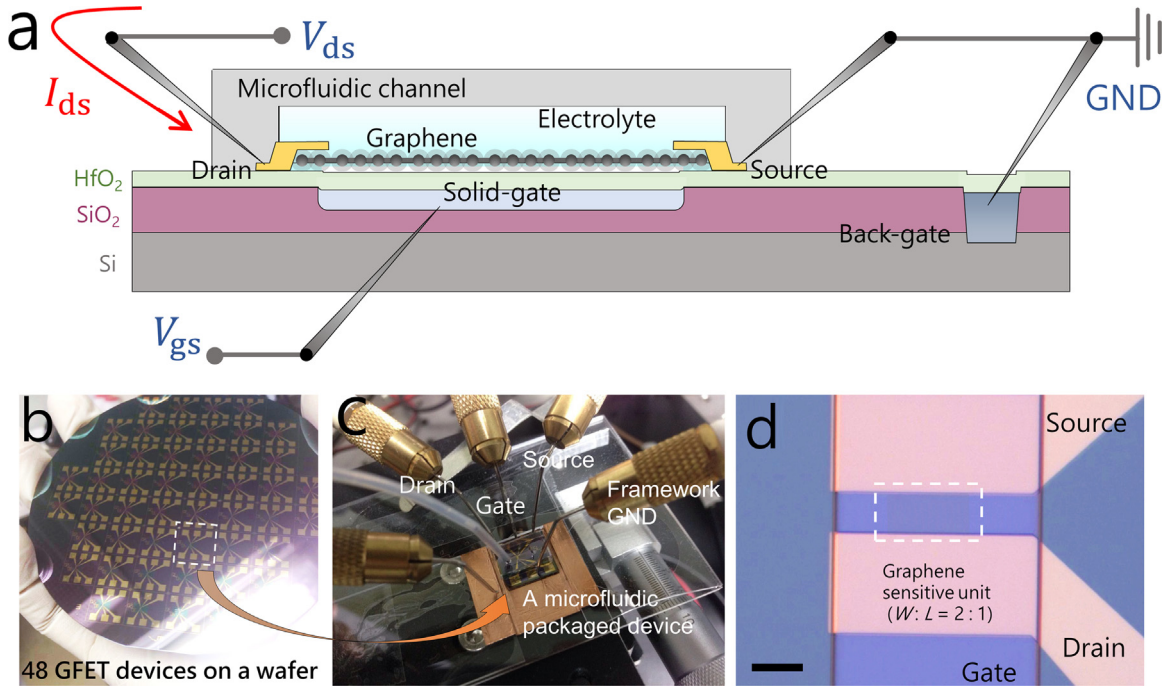

Fig. 1. GFET electronic sensor device. (a) Device and test circuitry schematics. (b) A batch of 48 GFET devices integrated on a 4-in. wafer. (c) A microfluidic channel packaged sensor device in experiment. (d) Optical micrograph of the rectangle graphene sensitive unit with width 80 μm and length 40 μm (scale bar is 50 μm).

also via electric field-effect. Then, after a HEPES buffer rinsing lasting 1 h, a *p*-type doping recovery $V^{(v)}_{Dirac} = 1.627$ V, almost identical to $V^{(iii)}_{Dirac}$, illustrates the reversibility of DexAgNP-ConA affinity (stage v). Meanwhile, the time-resolved responses during the HEPES rinsing (observed at $V_{gs} = 1.5$ V) are plotted in Fig. 3**b**. The decreasing and asymptotically saturating kinetics suggest a complete release of DexAgNPs. Altogether these results verify the electronic signaling capability of DexAgNPs, and the reversible DexAgNP-ConA affinity can be exploited to competitively enable the electronic signaling of glucose recognition.

However, before the glucose bioassay demonstration in order, the DexAgNP-induced *n*-type doping (from stage iii to iv in Fig. 3**a**) greatly attracts our interests. As our preliminary quality characterization of DexAgNPs (SI Fig. S5a) indicated a negative zeta-potential $\xi \approx -25$ mV (in HEPES buffer, pH = 7.4, $I \approx 50$ mM), the *n*-type doping result is contrary to the conventional viewpoint that negative charges accumulating nearby the biointerface may induce opposite *p*-type doping (Lerner et al., 2014; Saltzgaber et al., 2013). This conflict probably implies an unexplored electronic signaling mechanism of the metal nanoparticle analogue rather than simplistic charge accumulation.

To fundamentally set forth this newly observed electronic signaling mechanism and confirm the competitive affinity sensing principle, it would be necessary to quantitatively discuss the interfacial bioelectronic behaviors with respect to the DexAgNP-ConA affinity. Herein, we established an electrical analysis approach based on the equivalent circuit of our GFET electronic biosensor in Fig. 3**c**(Wang et al., 2016). At an observation point V_{gs}, the carrier equilibrium in graphene (usually represented by chemical potential V_{ch}) is constrained by the capacitive network consisting of a solid-gate capacitance C_{sol}, a quantum

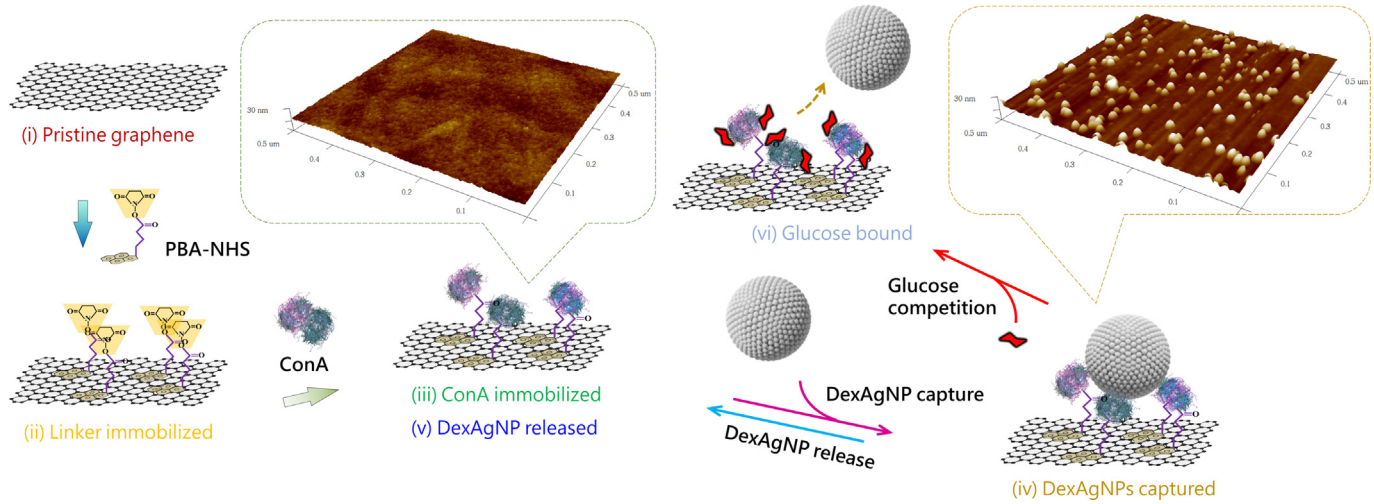

Fig. 2. Competitive affinity biosensing principle of glucose assisted by DexAgNP analogue. To achieve glucose recognition, pristine graphene sensitive unit (stage i) is functionalized by PBA-NHS (stage ii), and ConA receptor (stage iii) in order. Reversible capture (stage iv) and release (stage v) of DexAgNP analogue on ConA enable electronic signaling. In presence of glucose, glucose-ConA affinity may competitively accelerate DexAgNP release process (stage vi), and transduce glucose concentration information into electronic responses.

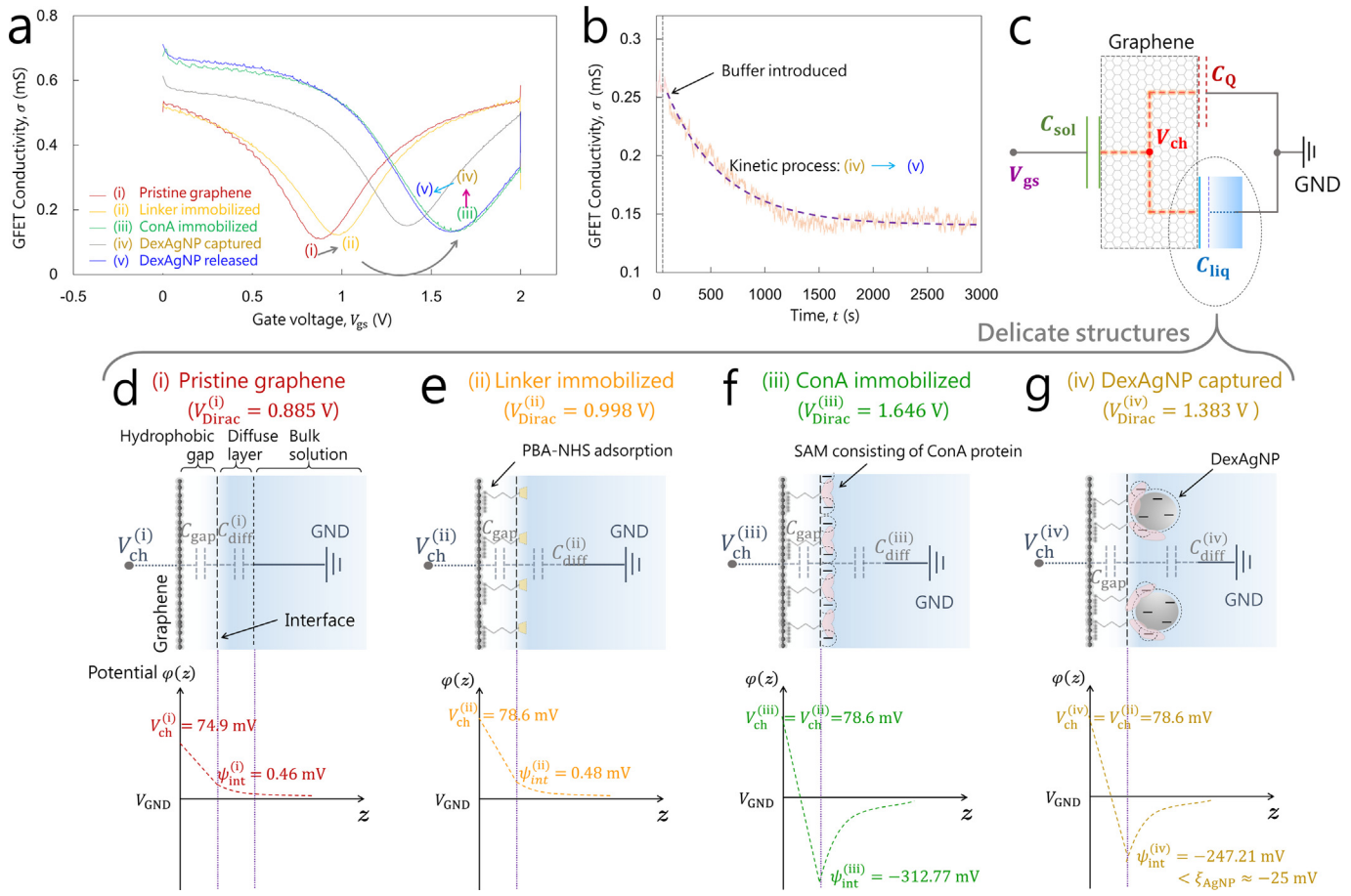

Fig. 3. Quantitative analysis of potential distribution in GFET biosensor. (a) GFET transfer characteristic curves of stages i – v (measured at drain bias V_{ds} = 20 mV). (b) Kinetic process of the DexAgNP release in buffer solution without glucose competition (from stage iv to v). (c) Capacitive equivalent circuit of GFET biosensor. (d) – (g) Delicate C_{liq} structures and inside potential distributions of stages i – iv. Dashed circles in (f) and (g) qualitatively represent Debye screening length of charges in buffer solution.

capacitance C_Q correlative with V_{ch}, and an electrical double layer (EDL) capacitance C_{liq}. In the delicate structure of C_{liq} (Fig. 3**d – g**), the graphene-solution interfacial potential ψ_{int}, which applies electric field-effect on the hydrophobic gap capacitance C_{gap} to alter V_{ch}, is a critical parameter directly reflecting the electrical potential impacts from the adjacent ConA receptor and DexAgNP analogue. Consider that the electric filed-induced carriers are depleted at Dirac voltage $V_{gs} = V_{Dirac}$, and the remnant carriers are only supplied by impurity-led puddles (Chen et al., 2008), the V_{Dirac} shifts in Fig. 3**a** reflect the electric field-effect compensations with respect to ψ_{int} variations (Meric et al., 2008). On the basis of this theory, we quantitatively estimated the ψ_{int} values stage-by-stage at corresponding V_{Dirac} points to reveal the electronic signaling mechanism of DexAgNPs.

The detailed theoretical derivation and calculation results are provided in SI Fig. S6, S7 and Table S1. First, in the situations devoid of charged SAM in the vicinity of graphene-solution interface (i.e., stages i and ii), the graphene chemical potential V_{ch} can be directly calculated (Fig. S6). In stage i, $V^{(i)}_{ch}$ = 74.9 mV is estimated at the gate voltage $V_{gs} = V^{(i)}_{Dirac}$ = 0.885 V, and the interfacial potential is extracted as $\psi^{(i)}_{int}$ = 0.46 mV (Fig. 3**d**). Similarly, in stage ii, $V^{(ii)}_{ch}$ = 78.6 mV and $\psi^{(ii)}_{int}$ = 0.48 mV are solved at $V_{gs} = V^{(ii)}_{Dirac}$ = 0.998 V (Fig. 3**e**). The result $V^{(i)}_{ch} < V^{(ii)}_{ch}$ indicates a slight increase of *p*-type doping, in agreement with the shift of Dirac voltage identifier $V^{(i)}_{Dirac} < V^{(ii)}_{Dirac}$, which suggests a few incidental impurities from the PBA-NHS linker adsorption. And due to the missing of charged SAM, the interfacial potential values $\psi^{(i)}_{int}$ and $\psi^{(ii)}_{int}$ are quite low. Next, in stage iii, ConA protein molecules compactly arranged nearby the graphene-solution interface form a charged SAM (Fig. S7). Since ConA is anchored by PBA-NHS linker without direct contacting on graphene, the density of non-depletable puddle carriers may remain identical to stage ii (Fig. 3**f**). Therefore, the gate-adjustment $V_{gs} = V^{(iii)}_{Dirac}$ = 1.646 V may compensate the SAM impact via electric field-effect and maintain the graphene chemical potential in constant $V^{(iii)}_{ch} = V^{(ii)}_{ch}$ = 78.6 mV. And the interfacial potential reflecting the negative potential propagating from SAM (Fig. 3**f**) is solved as $\psi^{(iii)}_{int}$ = -312.77 mV. Furthermore, in stage iv, the DexAgNP-ConA affinity on SAM also fulfills the noncontact condition. Therefore, at $V_{gs} = V^{(iv)}_{Dirac}$ = 1.383 V, the graphene chemical potential $V^{(iv)}_{ch} = V^{(ii)}_{ch}$ = 78.6 mV may remain in constant, and $\psi^{(iv)}_{int}$ = -247.21 mV is correspondingly solved (Fig. 3**g**). The result $\psi^{(iv)}_{int} > \psi^{(iii)}_{int}$ indicates an inhibition in the interfacial potential negativity with respect to the DexAgNP-ConA affinity, although the DexAgNPs are also negatively charged. By recalling the zeta-potential of DexAgNPs $\xi \approx$ -25 mV, much less negative than $\psi^{(iii)}_{int}$ = -312.77 mV, we hereby attribute the electronic signaling mechanism as the electrostatic shielding-effect (Molinaro et al., 2016). The captured DexAgNPs as equipotential metallic conductors with tenuous charge density may disperse ConA charges, and thus reduce the collective potential of SAM (Scanlon et al., 2015). This elucidation is also supported by the zeta-potential characterization of ConA-wrapped DexAgNPs, as an imitation of DexAgNP-ConA affinity, in which the zeta-potential change from a few bound ConA molecules is measured to be negligible (SI Fig. S5b).

To further supply solid experimental evidence of the electrostatic shielding-effect, and the electronic signaling capability as well, we carried out a KPFM characterization to measure the surface potential

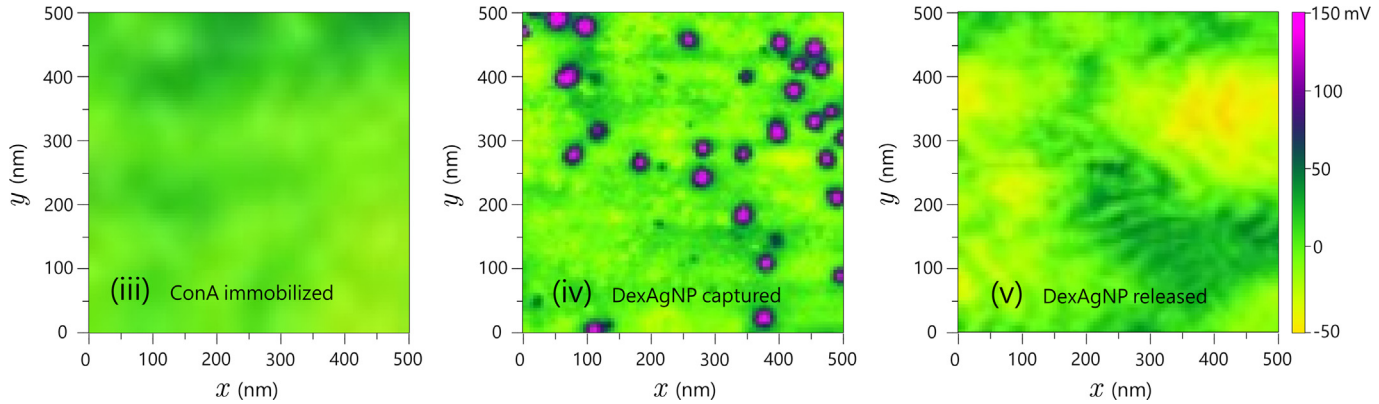

Fig. 4. KPFM-characterized surface electrical potential distributions with respect to the reversible DexAgNP-ConA affinity in GFET biosensor.

variations with respect to the capture and release of DexAgNPs. As shown in Fig. 4, the SAM potential in stage iii is set as the reference (green background). In stage iv, the captured DexAgNPs (magenta circles) exhibit a perspicuous potential contrast about 150 mV less negative. Thus, the potential of ConA molecules beneath DexAgNPs should be shielded and effectively lower the overall potential of SAM. While DexAgNPs are released in stage v, the SAM potential basically recovers. In short, the electronic signaling in affinity biosensing can be enabled as long as the interfacial potential ψ_{int} is altered, no matter strengthened or suppressed.

2.4. Biosensing verification

While the electronic signaling mechanism has been set forth, the glucose bioassay was executed as the proof-of-principle of competitive affinity small-molecule biosensing (stage iv to vi in Fig. 2**a**). As the equivalent electrical schematic and GFET energy bands diagram of glucose biosensing shown in Fig. 5**a**, before the glucose presence, the negative ConA charges are partially shielded by DexAgNPs. While the competition happens, uncharged glucose molecules kinetically occupy ConA binding sites and release DexAgNPs into bulk solution. Thus, the disappearance of electrostatic shielding-effect may result in a *p*-type doping recovery of GFET. As the process of DexAgNP release might be accelerated by the competition, the glucose concentration could be quantified by observing the GFET kinetics over time. We then conducted the detection of glucose samples at various concentrations (0–50 μg dL^{-1}), and recorded the time-resolved responses via continuous amperometric measurement of I_{gs}.

The complete experimental dataset of glucose sensing verification is provided in SI Figs. S8 – S17. To confirm the sensing reproducibility, each glucose sample at a particular concentration was measured in triplicates. And each measurement used an individual device as disposable sensor. As shown in the subfigures of SI Figs. S8 – S17, all the response processes perform stable kinetic characteristics in nearly an hour, which preserve the reliable stability of electrical measurements for long-time electronic biosensing. Moreover, in the triplicated detections of a glucose sample, 3 batch-made devices with similar electrical characteristics perform high reproducibility in the time-resolved responses. Although not completely identical to each other, the device-to-device nonuniformity can be further minimized via a regular signal processing of normalization (Homola, 2008). By normalizing the time-resolved responses into universal kinetic proceeding processes (see the double-ordinate subfigures in SI Fig. S8 – S17 for normalization method), the saturation rate seems to be uniform and proportional to the glucose concentration. As shown in Fig. 5**b**, the normalized response process of 50 μg dL^{-1} glucose sample, which is selected from SI Fig. S8 as a representative, indicates a rapid saturation in 1 min. For the 10 μg dL^{-1} sample, a prolonged competition time lasting 5 min is required (Fig. 5**c**). These results illustrate the acceleration in DexAgNP release under the glucose competition. To prevent the errors caused by the saturation of kinetic responses, the normalized responses observed at t = 60 s are plotted in the glucose concentration range 0 – 50 μg dL^{-1} (Fig. 5**d**). Based on the sensitivity S^{60} = 0.0163 dL μg^{-1} and the standard deviation σ^{60} = 0.051 provided by the linear calibration curve (see numerical statistics in SI Table S2), the limit of detection (LOD) is estimated as: LOD^{60} = $3\sigma^{60}/S^{60}$ = 9.4 μg dL^{-1}. Similarly, for the lower concentrated glucose samples (0 – 10 μg dL^{-1}), the normalized responses observed at t = 300 s supplies an enhanced sensitivity S^{300} = 0.0543 dL μg^{-1} (Fig. 5**e**). By using σ^{300} = 0.054, the LOD is improved to: LOD^{300} = $3\sigma^{300}/S^{300}$ = 3.0 μg dL^{-1} (ca. 165.3 nM). As a representative proof-of-principle, the LOD of glucose concentration four orders of magnitude lower than the regular human blood sugar level verifies the electronic signaling capability of metal nanoparticles based on the electrostatic shield-effect, which performs even better than most of commercial glucometer settings.

Furthermore, to confirm the principle generality of the nanoparticle-enabled competitive affinity biosensing, we conducted an additional bioassay of fructose. As shown in SI Figs. S18, the target analyte fructose possessing similar ConA-binding sites also exhibits positive results. The responses dependent to fructose concentrations perform the sensitivity parameters S^{60} = 0.0205 dL μg^{-1} and S^{300} = 0.0516 dL μg^{-1}, respectively (SI Figs. S18j), which are close to the competition results of glucose (Fig. 5**d and e**). In contrary, galactose without ConA-binding capability exhibits negative results as shown in SI Figs. S19 and S20. Either varying in concentration or mixed into glucose samples as a disruptor, galactose does not lead to any significant impact. On the basis of the results of positive and negative control experiments, we summarize that the electronic signaling principle based on electrostatic shielding-effect is generally applicable, only if the epitope-modified metal nanoparticle analogue binding on receptor can be competitively released by the small molecule affinity.

In addition to the proof-of-principle, we also estimate that the metal nanoparticle-enabled competitive affinity biosensing incorporated in our GFET devices may realize a scenario of disposable biosensors competent to practical applications. Owing to the standard IC fabrication techniques appropriate for the scalable integration of devices, our GFET devices are technically capable of the large-scale manufacture with high yield. Although the current device size 1 cm × 1 cm only achieves 48 devices integrated on a wafer (Fig. 1**b**), without changing the key graphene sensitive unit (80 μm × 40 μm), the scale-down of overall device size for a higher integration level may reduce the fabrication cost. We conservatively estimate that the cost of an individual device could be lowered under 2 USD, based on the current fabrication technology conditions.

3. Conclusion

In summary, we presented a novel analogue made by epitope-

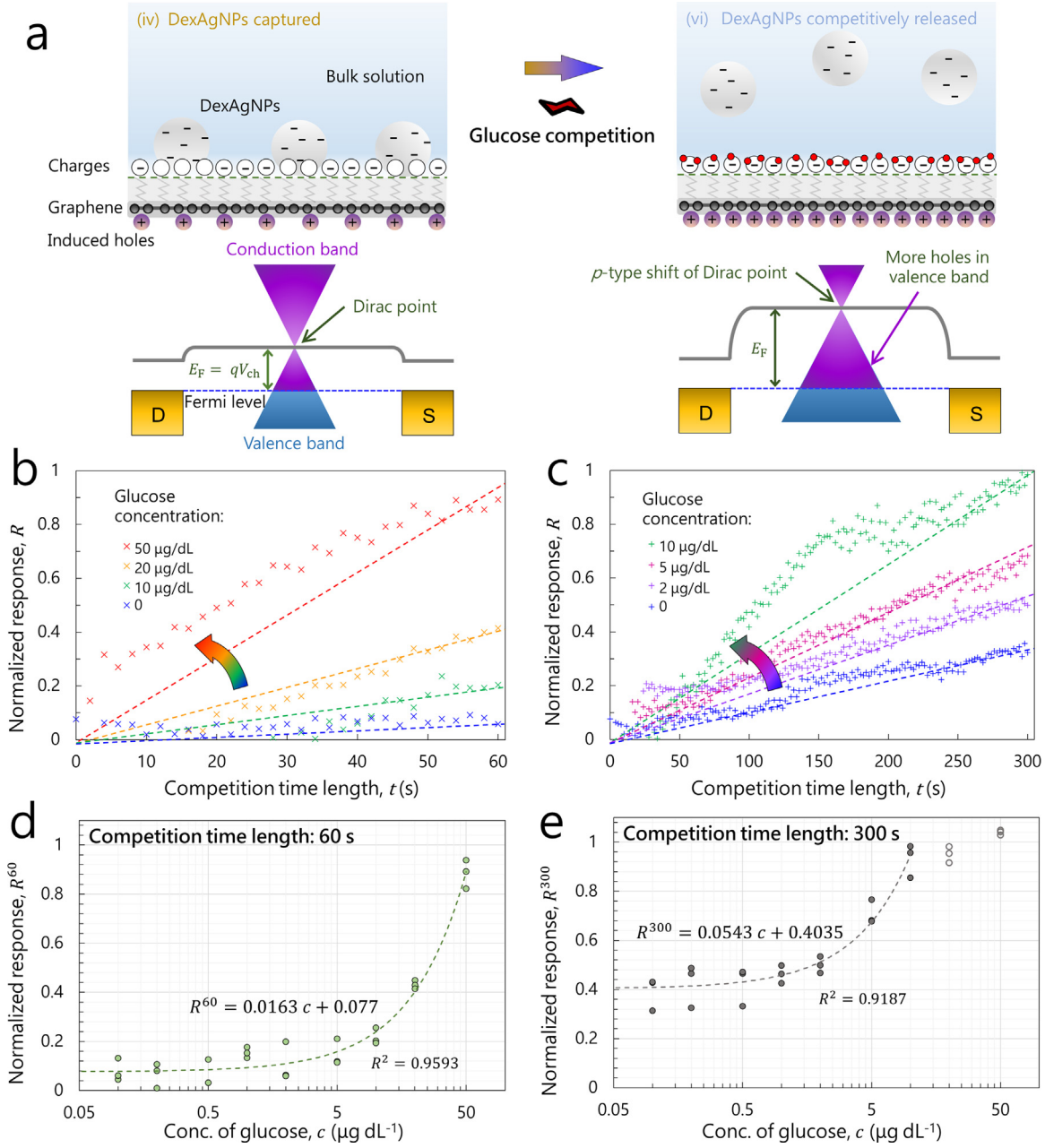

Fig. 5. DexAgNP-enabled competitive affinity electronic biosensing of glucose based on GFET. (a) Equivalent electrical schematic of the competitive affinity GFET biosensing and corresponding energy bands diagram. (b) Representative normalized responses of 60-s glucose sensing kinetics (cut out from SI Fig. S8a, S15a, S16a and S17a). (c) Representative normalized responses of 300-s glucose sensing kinetics (cut out from SI Fig. S8a, S13a, S14a and S15a). (d) – (e) Normalized responses of various glucose concentrations observed at (d) t = 60 s and (e) t = 300 s (under gate voltage V_{gs} = 1 V). The concentration-dependent relationships are fitted by the dash lines indicating empirical linear calibration curves.

modified metal nanoparticles to facilitate the competitive affinity electronic biosensing of uncharged analytes. By performing a GFET bioassay of small-molecule glucose as a representative, we verified the utility of metal nanoparticle analogue, and fundamentally elucidated the electronic signaling mechanism as the electrostatic shielding-effect. Further consider the innate modifiability, metal nanoparticles with proper epitope-modifications may open up the facile analogue customization for the competitive affinity electronic biosensing of range-extended small molecules based on the electrostatic shield-effect. Following this perspective, more label-free electronic biosensors and future practical applications without reliance on sophisticated analytical instruments are looking forward.

Acknowledgements

The authors are grateful to the Technology Research & Development Program of Guangxi Zhuang Autonomous Region, China (AB17129007), the Natural Science Foundation of Tianjin City, China (18JCYBJC86000), the Funding Program of Tianjin Higher Education Creative Team and the Science & Technology Development Fund of Tianjin Education Commission for Higher Education, China (2018KJ153) for funding this work. C.W. acknowledges the Distinguished Young Talent Recruitment Program of Tianjin Normal University, China (011/5RL153). W.Y. acknowledges the MAINZ Excellence Initiative Fellowship, Germany (GSC266).

Declaration of interests

The authors declare no competing interests.

CRediT authorship contribution statement

Cheng Wang: Conceptualization, Investigation, Project administration. **Weixiang Ye:** Conceptualization, Investigation. **Yijun Li:** Investigation, Resources. **Yibo Zhu:** Formal analysis, Resources. **Qiao Lin:** Formal analysis, Supervision. **Miao He:** Conceptualization, Funding acquisition, Supervision.

Appendix A. Supporting information

Supplementary data associated with this article can be found in the online version at https://doi.org/10.1016/j.bios.2018.12.051.

References

Chen, J.-H., Jang, C., Xiao, S., Ishigami, M., Fuhrer, M.S., 2008. Nat. Nanotechnol. 3 (4), 206–209.
Cummins, B.M., Garza, J.T., Coté, G.L., 2013. Anal. Chem. 85 (11), 5397.
Fu, W., Jiang, L., van Geest, E.P., Lima, L., Schneider, G.F., 2016. Adv. Mater. 29 (6), 1603610.
Homola, J., 2008. Chem. Rev. 108 (2), 462–493.
Lerner, M.B., Matsunaga, F., Han, G.H., Hong, S.J., Xi, J., Crook, A., Perez-Aguilar, J.M., Park, Y.W., Saven, J.G., Liu, R., Johnson, A.T.C., 2014. Nano Lett. 14 (5), 2709–2714.
Li, Y., Wang, C., Zhu, Y., Zhou, X., Xiang, Y., He, M., Zeng, S., 2017. Biosens. Bioelectron. 89, 758–763.
Li, Y., Zhu, Y., Wang, C., He, M., Lin, Q., 2019. Biosens. Bioelectron. 126, 59–67.
Locke, A.K., Cummins, B.M., Abraham, A.A., Cote, G.L., 2014. Anal. Chem. 86 (18), 9091–9097.
Loka, R.S., McConnell, M.S., Nguyen, H.M., 2015. Biomacromolecules 16 (12), 4013–4021.
Luo, X., Davis, J.J., 2013. Chem. Soc. Rev. 42 (13), 5944–5962.
Meric, I., Han, M.Y., Young, A.F., Ozyilmaz, B., Kim, P., Shepard, K.L., 2008. Nat. Nanotechnol. 3 (11), 654–659.
Molinaro, R., Corbo, C., Martinez, J.O., Taraballi, F., Evangelopoulos, M., Minardi, S., Yazdi, I.K., Zhao, P., De Rosa, E., Sherman, M., De Vita, A., Toledano Furman, N.E., Wang, X., Parodi, A., Tasciotti, E., 2016. Nat. Mater. 15 (9), 1037.
Novoselov, K.S., Fal, V., Colombo, L., Gellert, P., Schwab, M., Kim, K., 2012. Nature 490 (7419), 192–200.
Pace, C.N., Grimsley, G.R., Scholtz, J.M., 2009. J. Biol. Chem. 284 (20), 13285–13289.
Saltzgaber, G., Wojcik, P., Sharf, T., Leyden, M.R., Wardini, J.L., Heist, C.A., Adenuga, A.A., Remcho, V.T., Minot, E.D., 2013. Nanotechnology 24 (35), 355502.
Scanlon, M.D., Peljo, P., Méndez, M.A., Smirnov, E., Girault, H.H., 2015. Chem. Sci. 6 (5), 2705–2720.
Sperling, R.A., Parak, W., 2010. Philos. Trans. R. Soc. A 368 (1915), 1333–1383.
Sreeprasad, T., Berry, V., 2013. Small 9 (3), 341–350.
Wang, C., Kim, J., Zhu, Y., Yang, J., Lee, G.-H., Lee, S., Yu, J., Pei, R., Liu, G., Nuckolls, C., Hone, J., Lin, Q., 2015. Biosens. Bioelectron. 71, 222–229.
Wang, C., Li, Y., Zhu, Y., Zhou, X., Lin, Q., He, M., 2016. Adv. Funct. Mater. 26 (42), 7668–7678.
Wang, C., Zhang, W., Li, W., Liu, R., Liu, G., 2014. Micro Nano Lett. 9 (5), 320–324.
Ye, W., Zhang, W., Wang, C., Li, W., Yu, H., Liu, G., 2014. Micro Nano Lett. 9 (4), 294–296.
Zayats, M., Huang, Y., Gill, R., Ma, C.-A., Willner, I., 2006. J. Am. Chem. Soc. 128 (42), 13666–13667.
Zeng, S., Baillargeat, D., Ho, H.-P., Yong, K.-T., 2014. Chem. Soc. Rev. 43 (10), 3426–3452.
Zhang, A., Lieber, C.M., 2015. Chem. Rev. 116 (1), 215–257.
Zhang, W., Ye, W., Wang, C., Li, W., Yue, Z., Liu, G., 2014. Micro Nano Lett. 9 (9), 585–587.
Zhu, Y., Wang, C., Petrone, N., Yu, J., Nuckolls, C., Hone, J., Lin, Q., 2015. Appl. Phys. Lett. 106 (12), 123503.